

Supplementary material for

**Strongly adsorbent rough surface induced rapid  
hydrolysis of cellulose to sugar in the aqueous phase**

*Chengqi Feng<sup>a</sup>, Hong Liu<sup>a,b</sup>, Chenkai Jin<sup>a</sup>, Jinhang Yang<sup>a,b</sup>, Yifei Huang<sup>a,b</sup>,*

*Juncheng Huang<sup>a</sup>, Haining Na<sup>\*,a,b</sup> and Jin Zhu<sup>\*,a</sup>*

[<sup>a</sup>] Key Laboratory of Bio-Based Polymeric Materials of Zhejiang Province, Ningbo  
Institute of Materials Technology and Engineering, Chinese Academy of Sciences,  
Ningbo, Zhejiang 315201, China;

[<sup>b</sup>] University of Chinese Academy of Sciences, Beijing 100049, China.

\*Corresponding Author: Dr. Haining Na (*nahaining@nimte.ac.cn*)

Dr. Jin Zhu (*jzhu@nimte.ac.cn*)

Tel: +86-574-86693591, Fax: +86-574-86685186

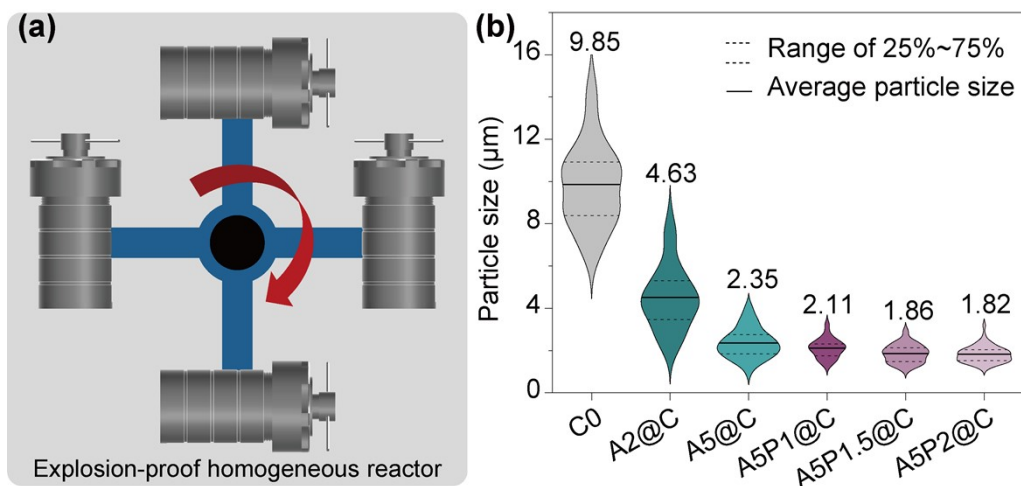


Figure S1. (a) Forms of rotation of high-pressure reactors in this work; (b) The particle size distribution and average particle size of catalysts (A10@C could not be pelletized during the hydrothermal process; no information on particle size distribution was compiled).

Nano Measurer 1.2 was utilized to perform particle size statistics on SEM images of solid acids, with a minimum sample size of 50 for each solid acid. The sample particle size data were obtained for particle size distribution mapping.

### **Obtaining surface roughness Ra:**

The average surface roughness (Ra) is the centerline average or arithmetic mean. It is the average roughness between the roughness curve and the mean line and is a standard metric for quantifying roughness.

The solid acids we worked with had particle sizes between 4.63 and 1.82  $\mu\text{m}$ . Unfortunately, this particle size range is beyond the optimal operating range of the AFM, and the large up and down fluctuations of the voltage signal make it challenging to stabilize the voltage signal to quantify the surface roughness of the solid acids accurately. 3D Profiler and laser confocal microscope are challenging to achieve sufficient resolution to quantify solid acid roughness. Therefore, it needs to be measured by indirect methods.

Figure S2a shows that the solid acid has an overall spherical shape and a relatively uniform surface roughness as observed by SEM, which means that the morphology curve obtained by scanning through path B using AFM is similar to that obtained by observing the hemispherical edge projection (curve A) through SEM, and both of them can be used to characterize the roughness of the surface of the solid acid. Therefore, after an in-depth discussion, we decided to quantify the roughness of the solid acid using the edge projection corresponding to A. The specific operation steps are as follows:

- (1). Open the SEM image with PS, select the color scale tool, and set the input and output color scale to 126 and 128, respectively, to convert the image to only black and white (Figure S2c).

- (2). The outline of the black and white pictures was red by ImageJ, and the outline picture (Figure S2d).
- (3). The contours in the picture were converted into data points by Origin and saved the data (Figure S2e).
- (4). Ra was calculated (Figure S2f).

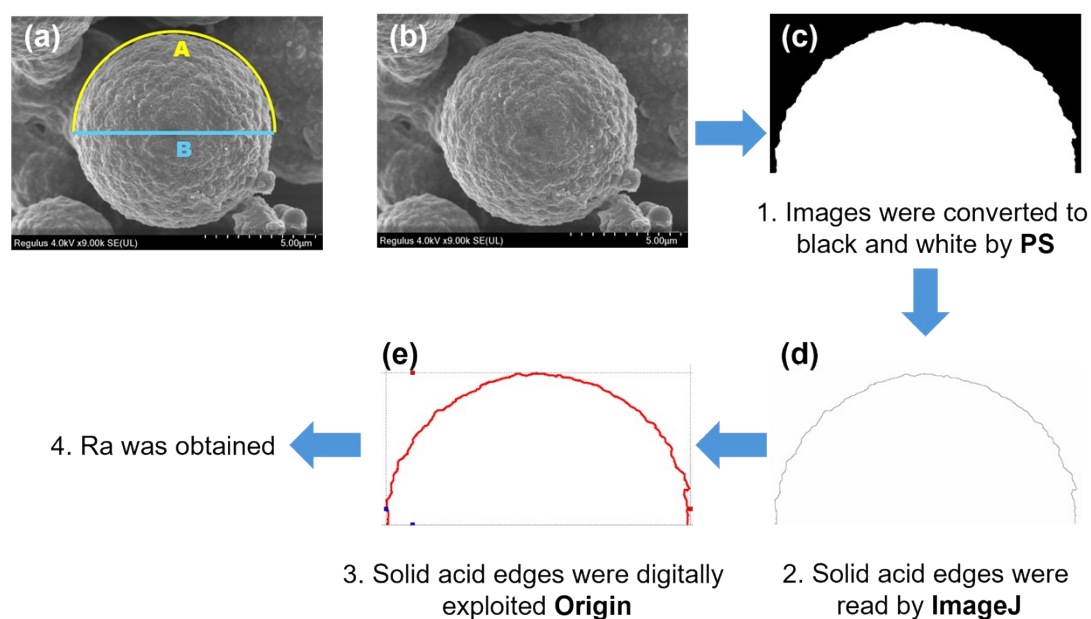


Figure S2. Process of calculating surface roughness of solid acid. (a) Schematic of AFM scanning and SEM observation of edge paths; (b) SEM image of solid acid; (c) Black and white color map of solid acid; (d) Solid acid edges; (e) Digitization of solid acid edges; (f) Ra was calculated.

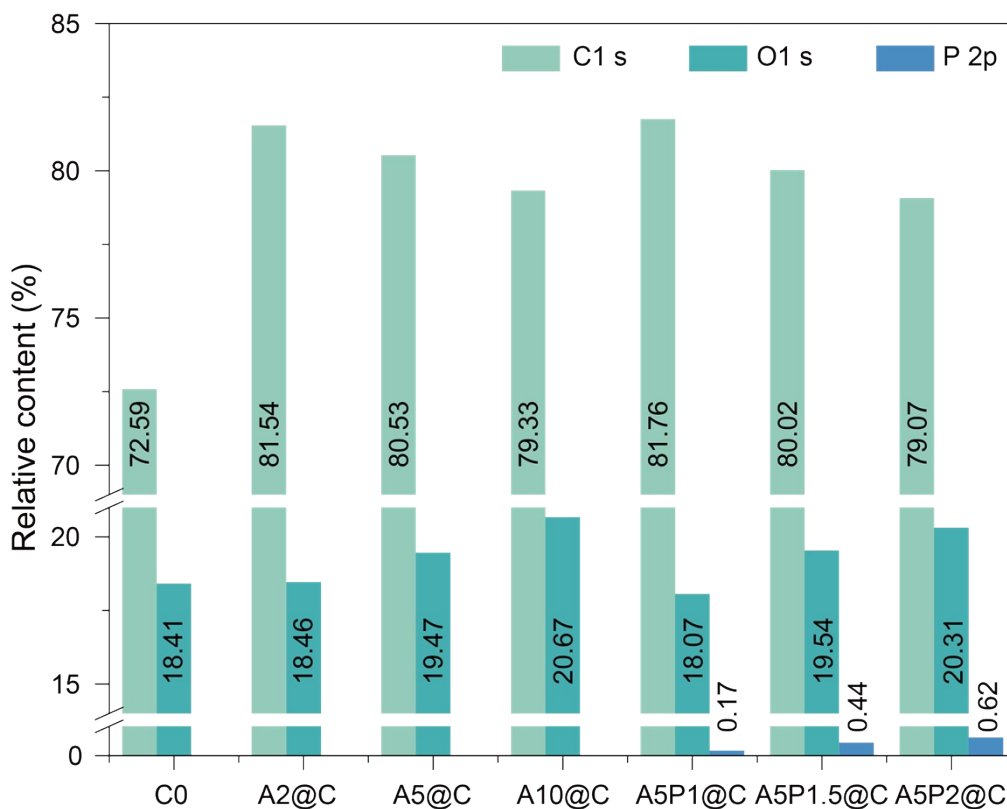


Figure S3. Detection of surface elemental content of solid acids by XPS.

It can be seen in Figure S1 that the solid acids all contain C 1s and O 1s peaks. Compared with C0, the solid acids, after adding acrylic acid, have higher oxygen content, and the O elemental content increases when the acrylic acid content increases. Among them, A10@C has the highest oxygen content (22.67%). It shows that adding acrylic acid effectively enhances the number of oxygen-containing functional groups on the surface of solid acids. When H<sub>3</sub>PO<sub>4</sub> was added to the system, the P element appeared on the surface of solid acid, and the content of the P element increased from 0.17% to 0.62% with the increase of H<sub>3</sub>PO<sub>4</sub> doping. The content of C and O elements was equal to A5@C.

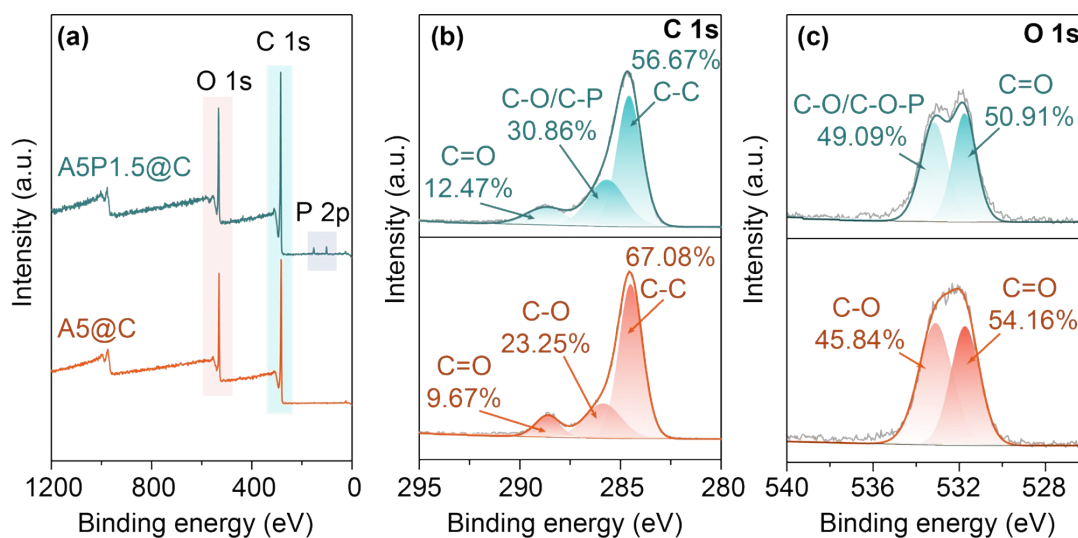


Figure S4. XPS analysis of A5P1.5@C and A5@C. (a) total spectrum; (b, c) solid acid C 1s and O 1s deconvolution profiles.

To further determine the content and distribution of functional groups on the catalyst surface, we performed peak splitting on the high-resolution exemplary spectrum of XPS, as shown in Figure S3. In C 1s, three peaks were detected, which were C-C (284.4 eV), C-O/C-P (286.3 eV), and C=O (288.6 eV) bonds, respectively<sup>1, 2</sup>. Two peaks in the O 1s spectrum appear at 531.5 eV and 533.2 eV, assigned to C=O and C-O, respectively<sup>3</sup>. After doping H<sub>3</sub>PO<sub>4</sub> in C 1s, the C-C bond content in A5P1.5@C decreased from 67.07% to 56.67%. And the relative content of C-O/C-O-P bonds increased from 23.25% to 30.86%. This implies that H<sub>3</sub>PO<sub>4</sub> is involved in constructing the solid acid skeleton to form C-O-P bonds.

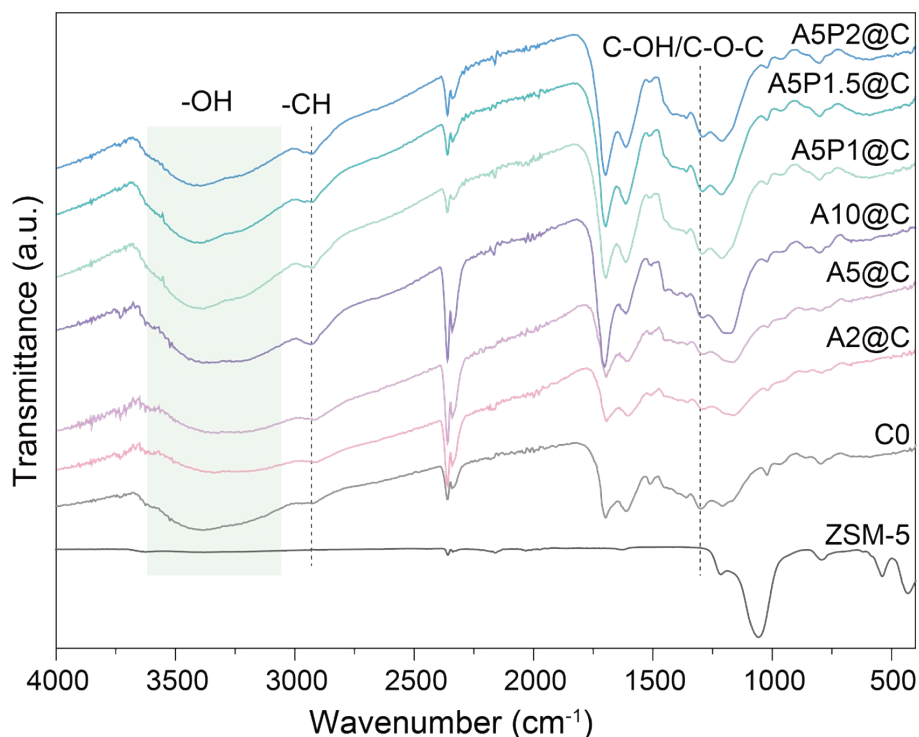


Figure S5. FT-IR spectra of solid acids.

Broad O-H stretching vibrations ( $3300\text{-}3550\text{ cm}^{-1}$ ) and C-OH bending vibrations ( $1011\text{-}1400\text{ cm}^{-1}$ ) were observed in the FT-IR spectra of all the solid acids, and the wider absorption bands emphasize a large amount of -OH, which in turn constitutes a hydrophilic carbon-based catalyst. The characteristic peak at  $2890\text{ cm}^{-1}$  is attributed to the stretching vibration of C-H. The FT-IR patterns of hydrothermal carbons show a stretching vibration peak of the C=O group at  $1700\text{ cm}^{-1}$ , indicating the presence of -COOH on the surface of all catalysts prepared by the hydrothermal method. The peak intensity liquid with increasing acrylic acid content implies that the increase can provide more surface-COOH to the catalysts. The characteristic peak at  $1643\text{ cm}^{-1}$  corresponded to the C=C backbone vibration in the aromatic ring. Glucose reacts with acrylic acid in a subcritical aqueous environment, such as dehydration and

condensation, and there is a prominent C=C structure in the catalyst backbone. When H<sub>3</sub>PO<sub>4</sub> was added to the system, the FT-IR pattern of the catalyst showed the prominent characteristic peaks of the phosphate group at 1213 cm<sup>-1</sup> and 1079 cm<sup>-1</sup>, corresponding to P=O, C-O/P-O, respectively <sup>4</sup>, which would increase the adsorption sites of the catalyst, and likewise improve its adsorption performance. It can be found that after doping with phosphoric acid, there is a broader absorption band at 592 cm<sup>-1</sup>, which is attributed to the C-P absorption peaks, which suggests that the phosphoric acid groups successfully participate in the reaction of the hydrothermal synthesis process by embedding inside the lattice through the cycloaddition reaction with HMF <sup>3</sup>.

To characterize the affinity of ZSM-5, C0, A5@C, and A5P1.5@C with cellulose, solid acid with cotton adsorption experiments were designed. Separately, 0.05 g of this solid acid was placed in 15 mL of deionized water and stirred for 3 h. Then, 0.1 g of cotton cellulose was placed in the solution and magnetically stirred at 25 °C. The results were shown in Figure S5.

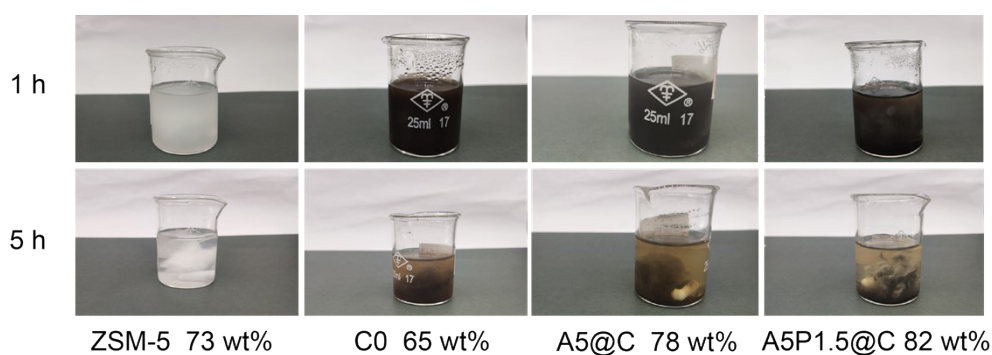


Figure S6. ZSM-5, C0, A5@C, and A5P1.5@C adsorption properties on cotton cellulose at different times.

The results showed that after 1 h of magnetic stirring, cotton cellulose was only slightly visible in the C-2AA solution and C-5AA solution, which indicated that the adsorption rate of cotton cellulose was faster. The other solutions were still in the turbid state. Cotton cellulose could be observed after 5 h of stirring except in the C-5AA solution. Further quantitative calculations were carried out, and it was found that the porous structure enhanced the adsorption performance of ZSM-5 after 5 h (73 wt%), which was higher than that of C0 (65 wt%). The adsorption of cotton cellulose by A5@C when adding acrylic acid amounted to 78 wt%, respectively, attributed to the rough surface and the elevated number of oxygen-containing functional groups. The adsorption of A5P1.5@C was further enhanced to 82 wt% after doping with H<sub>3</sub>PO<sub>4</sub>.

This results from the topological surface and the further enhancement of oxygen-containing functional groups.

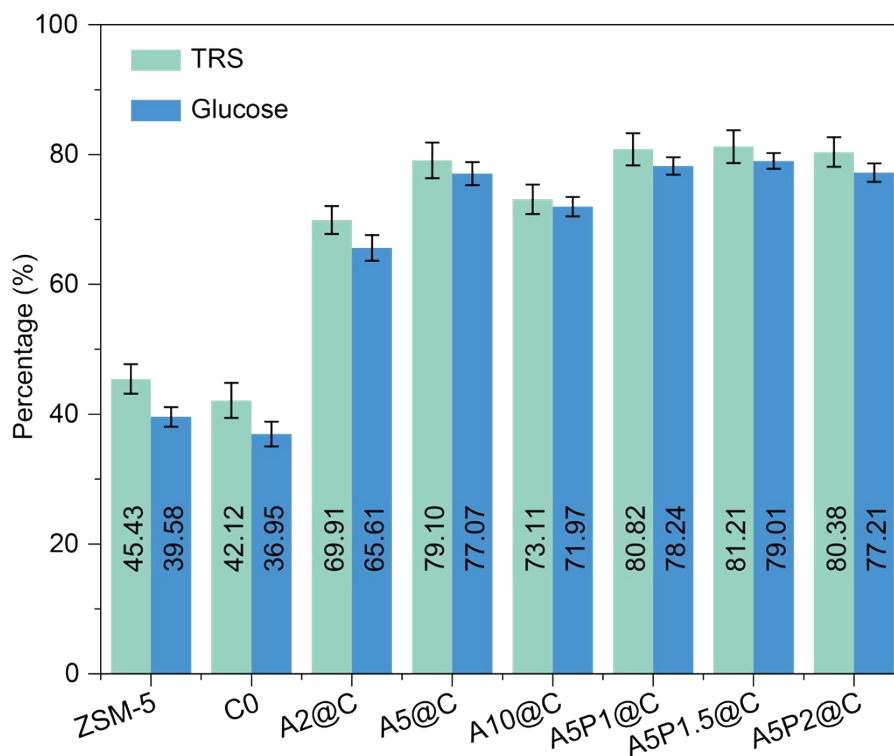


Figure S7. TRS and glucose yield in the hydrolysate after secondary hydrolysis.

The yield of TRS in the hydrolysate was much higher than that of glucose, probably because the hydrolysate contained incompletely hydrolyzed soluble oligoglucose (DP of 2-10). Therefore, the hydrolysate was processed secondarily to accurately demonstrate the catalytic performance of the solid acids <sup>5</sup>, as shown in Fig. S 5. After the secondary hydrolysis, all catalysts' TRS and glucose yield were improved. TRS and glucose yields in A5P1.5@C reached 81.21% and 79.01%, respectively. This indicates the presence of oligosaccharides in the hydrolysate.

Table S1 Effect of hydrolysis by solid acid (A5P1.5@C) compared with published work.

<b>Type</b>	<b>TRS yield (%)</b>	<b>Glucose yield (%)</b>	<b>Ref</b>
H-form zeolites	17.8	11.2	6
Metal oxide	8.5	0.8	7
Supported metal	46.8	34.2	8
Inorganic-organic composite	51	42	9
SO <sub>3</sub> H-based polymers	5.3	1.4	10
	26	11	11
Sulfonated carbonaceous solid acids	64	4	12
	42.5	40.5	6
	74.3	62.6	13
Un sulfonated carbonaceous solid acids	91	20	14
	26	2	15
	54	35	16
Magnetically recoverable solid acids	48.6	25.3	17
<b>This work</b>	<b>83.67</b>	<b>65.29</b>	

## References

1. A. M. Puziy, O. I. Poddubnaya and A. M. Ziatdinov, *Applied Surface Science*, 2006, **252**, 8036-8038. <https://doi.org/10.1016/j.apsusc.2005.10.044>.
2. D. J. Morgan, *C*, 2021, **7**, 51. <https://doi.org/10.3390/c7030051>.
3. Y. Dai, M. Geng, Y. Tao, Z. Zhang, C. Feng, J. Huang, F. Liu, H. Na and J. Zhu, *Carbon*, 2023, **206**, 72-83. <https://doi.org/10.1016/j.carbon.2023.02.006>.
4. M. A. Patel, F. Luo, M. R. Khoshi, E. Rabie, Q. Zhang, C. R. Flach, R. Mendelsohn, E. Garfunkel, M. Szostak and H. He, *ACS Nano*, 2016, **10**, 2305-2315. <https://doi.org/10.1021/acsnano.5b07054>.
5. A. Sluiter, B. Hames, R. Ruiz, C. Scarlata, J. Sluiter, D. Templeton and D. Crocker, *Laboratory analytical procedure*, 2008, **1617**, 1-16.
6. A. Onda, T. Ochi and K. Yanagisawa, *Green Chemistry*, 2008, **10**, 1033-1037. <https://doi.org/10.1039/B808471H>.
7. A. Takagaki, C. Tagusagawa and K. Domen, *Chemical Communications*, 2008, DOI: 10.1039/B810346A, 5363-5365. <https://doi.org/10.1039/B810346A>.
8. H. Kobayashi, T. Komanoya, K. Hara and A. Fukuoka, *ChemSusChem*, 2010, **3**, 440-443. <https://doi.org/10.1002/cssc.200900296>.
9. S. Van de Vyver, L. Peng, J. Geboers, H. Schepers, F. de Clippel, C. J. Gommers, B. Goderis, P. A. Jacobs and B. F. Sels, *Green Chemistry*, 2010, **12**, 1560-1563. <https://doi.org/10.1039/c0gc00235f>.
10. G. Akiyama, R. Matsuda, H. Sato, M. Takata and S. Kitagawa, *Advanced*

- Materials*, 2011, **23**, 3294-3297. <https://doi.org/10.1002/adma.201101356>.
11. R. Rinaldi, R. Palkovits and F. Schüth, *Angewandte Chemie International Edition*, 2008, **47**, 8047-8050. <https://doi.org/10.1002/anie.200802879>.
12. S. Suganuma, K. Nakajima, M. Kitano, D. Yamaguchi, H. Kato, S. Hayashi and M. Hara, *Journal of the American Chemical Society*, 2008, **130**, 12787-12793. <https://doi.org/10.1021/ja803983h>.
13. J. Pang, A. Wang, M. Zheng and T. Zhang, *Chemical Communications*, 2010, **46**, 6935-6937. <https://doi.org/10.1039/c0cc02014a>.
14. H. Kobayashi, M. Yabushita, T. Komanoya, K. Hara, I. Fujita and A. Fukuoka, *ACS Catalysis*, 2013, **3**, 581-587. <https://doi.org/10.1021/cs300845f>.
15. G. S. Foo and C. Sievers, *ChemSusChem*, 2015, **8**, 534-543. <https://doi.org/10.1002/cssc.201402928>.
16. Y. Jiang, X. Li, X. Wang, L. Meng, H. Wang, G. Peng, X. Wang and X. Mu, *Green Chemistry*, 2012, **14**, 2162-2167. <https://doi.org/10.1039/C2GC35306G>.
17. C. Zhang, H. Wang, F. Liu, L. Wang and H. He, *Cellulose*, 2013, **20**, 127-134. <https://doi.org/10.1007/s10570-012-9839-5>.